Title

Silicon nanoporous membranes as a rigorous platform for validation of biomolecular transport models

Authors

Feinberg, Benjamin J
Hsiao, Jeff C
Park, Jaehyun
et al.

Publication Date

2017-08-01

DOI

10.1016/j.memsci.2017.04.030

Peer reviewed

HHS Public Access

Author manuscript

J Memb Sci. Author manuscript; available in PMC 2017 September 19.

Published in final edited form as:

J Memb Sci. 2017 August 15; 536: 44–51. doi:10.1016/j.memsci.2017.04.030.

Silicon nanoporous membranes as a rigorous platform for validation of biomolecular transport models

Benjamin J. Feinberg[1], **Jeff C. Hsiao**[1], **Jaehyun Park**[1], **Andrew L. Zydney**[2], **William H. Fissell**[3], and **Shuvo Roy**[1,*]

[1]Department of Bioengineering and Therapeutic Sciences, University of California, San Francisco, California, USA

[2]Department of Chemical Engineering, The Pennsylvania State University, University Park, PA

[3]Department of Medicine and Division of Nephrology and Hypertension, Vanderbilt University, Nashville, TN

Abstract

Microelectromechanical systems (MEMS), a technology that resulted from significant innovation in semiconductor fabrication, have recently been applied to the development of silicon nanopore membranes (SNM). In contrast to membranes fabricated from polymeric materials, SNM exhibit slit-shaped pores, monodisperse pore size, constant surface porosity, zero pore overlap, and sub-micron thickness. This development in membrane fabrication is applied herein for the validation of the XDLVO (extended Derjaguin, Landau, Verwey, and Overbeek) theory of membrane transport within the context of hemofiltration. In this work, the XDLVO model has been derived for the unique slit pore structure of SNM. Beta-2-microglobulin (B2M), a clinically relevant “middle molecular weight” solute in kidney disease, is highlighted in this study as the solute of interest. In order to determine interaction parameters within the XDLVO model for B2M and SNM, goniometric measurements were conducted, yielding a Hamaker constant of 4.61×10^{-21} J and an acid-base Gibbs free energy at contact of 41 mJ/m^2. The XDLVO model was combined with existing models for membrane sieving, with predictions of the refined model in good agreement with experimental data. Furthermore, the results show a significant difference between the XDLVO model and the simpler steric predictions typically applied in membrane transport. The refined model can be used as a tool to tailor membrane chemistry and maximize sieving or rejection of different biomolecules.

Keywords

Membrane transport; beta-2-microglobulin; XDLVO; MEMS; silicon nanopore membranes

*Corresponding author.

1. Introduction

Theoretical models for solvent and solute transport have been at the core of membrane science since the development of highly selective filtration membranes in the 1960s. These models, which have been summarized extensively in the literature [1], have been used to describe solute transport in a variety of membrane types and processes. Most models investigating solute sieving through membranes have focused on size-based (steric) and electrostatic (EL) interactions, and even in cases where models have been exhaustively fit to experimental data, numerous assumptions are required to describe data obtained with polymeric membranes due to the broad pore size distribution and irregular pore shape in most polymeric membranes [2][3][4]. Furthermore, the few studies investigating other interactions, such as Lifshitz van der Waals (LW) and acid-base (AB) interactions, have been only cursorily validated [5]. There is, therefore, a desire to fabricate a membrane with highly tunable, uniform pore geometry for investigating transport model variations more rigorously than is possible with polymeric membranes.

Most polymeric membranes are made by a phase-inversion process, resulting in non-uniform lateral and axial pore dimensions, with significant uncertainties (and spatial variability) in the active layer thickness, surface porosity, and pore tortuosity. This makes it impossible to quantitatively validate models describing the nanoscale interactions between solute and membrane during sieving. In order to limit the variability in these membrane parameters, investigations have been performed with “track etched” membranes introduced in the 1970s, with the results showing rough agreement with membrane transport models [6]. However, track etched membranes exhibit considerable limitations including variable pore number, inflexible pore design (with pore size greater than 15 nm), large thickness, and pore overlap [7].

Recently, silicon nanopore membranes (SNM) have been developed for use in numerous biomedical applications, including hemofiltration, the implantable renal assist device, the bioartificial pancreas, and extracorporeal membrane oxygenation [8][9][10]. SNM possess nearly monodisperse pore size and tunable pore geometry. Unlike other silicon membranes with sub-micron pores, which are made using a long and laborious focused ion-bean (FIB) drilling fabrication process [11][12], SNM can be fabricated relatively rapidly using microelectromechanical systems (MEMS) fabrication techniques. Importantly, SNM can be fabricated with a very thin membrane thickness (~200–500 nm) and zero pore overlap. Figure 1 depicts a plan-view scanning electron microscopy (SEM) image of the membrane pores. Details on the manufacture of SNM membranes are provided elsewhere [8].

The purpose of this work is to apply the precisely known membrane porosity and pore dimensions of SNM to rigorously investigate, within the context of hemofiltration, the transport of macromolecules through membrane pores. This includes the full spectrum of interactions between membrane and solute, including LW, AB, and EL contributions (collectively, the extended Derjaguin, Landau, Verwey, and Overbeek, or XDLVO, theory). While the SNM technology itself has been well-characterized previously, the application of SNM to membrane pore model validation represents a new and significant opportunity. As currently fabricated SNM have a slit pore design, we first derive the equations for the

interaction energy for a spherical solute in a slit pore and the osmotic reflection coefficient for slit pores in the following section. Since we are evaluating the validity of the XDLVO transport model from the perspective of kidney disease treatment, we select a clinically relevant middle molecular weight protein, Beta-2-microglobulin (B2M), as the solute of interest [13].

2. Model Formulation

2.1. General membrane transport equations

Solvent and mass transport through membranes can be determined by solving the relevant mass transfer equations. The rate of water transport, J_w, across the membrane can be written as

$$J_w = L_p\left(\Delta P - \sigma\Delta\pi\right) \quad \text{Eq 1}$$

where L_p is the hydraulic permeability of the membrane, ΔP is the hydraulic pressure difference across the membrane, $\Delta\pi$ is the osmotic pressure difference, and σ is the osmotic reflection coefficient. Mass transport through membrane pores is due to both convective and diffusive contributions. By solving the relevant differential mass transport equation across the membrane, the following is obtained for the actual sieving coefficient, S_a,

$$S_a = \frac{c_f}{c_{b,m}} = \frac{S_\infty exp\left(\mathrm{Pe}\right)}{S_\infty + exp\left(\mathrm{Pe}\right) - 1} \quad \text{Eq 2}$$

where c_f is the filtrate solute concentration, $c_{b,m}$ is the solute concentration in the feed solution at the membrane surface, S_∞ is the asymptotic sieving coefficient corresponding to convective transport alone, and Pe is the Peclet number, i.e. the ratio of convective to diffusive transport in the membrane [3]. The Peclet number itself can be calculated as

$$\mathrm{Pe} = \frac{J_w \delta_m S_\infty}{\varepsilon\phi K_d D_\infty} \quad \text{Eq 3}$$

where J_w is the water flux, δ_m is the membrane thickness, ε is membrane porosity, ϕ is the solute-membrane partition coefficient, K_d is the diffusive hindrance factor, and D_∞ is the bulk diffusion coefficient of the solute [3]. The asymptotic sieving coefficient, S_∞, is the sieving coefficient at very high Peclet number and is equal to the product of ϕ and the convective hindrance factor, K_c, i.e., $S_\infty = \phi K_c$.

Since it is difficult to experimentally determine the concentration of solute at the membrane surface, we define an observed sieving coefficient as

$$S_o = \frac{c_f}{c_{b,b}}. \quad \text{Eq 4}$$

where $c_{b,b}$ is the bulk concentration of solute in the feed solution. Through applying film theory and solving the differential equations for mass transfer across the feed-side boundary layer, we obtain

$$S_a = \frac{S_o}{(1 - S_o)\, exp\,(J_w/k_b) + S_o} \quad \text{Eq 5}$$

where k_b is the feed side external mass transfer coefficient, defined as $k_b = \mathrm{Sh} D_\infty / d_h$ where Sh is the Sherwood number and d_h is the hydraulic diameter of the flow channel [3]. For a long, thin rectangular channel, the Sherwood number can be approximated by [14],

$$\mathrm{Sh} = 1.65 \left(\mathrm{ReSc} \frac{d_h}{L} \right)^{0.33} \quad \text{Eq 6}$$

where Re = $\rho_s u_b d_h / \mu$ is the Reynolds number, i.e. the ratio of momentum forces to viscous forces, and Sc=$\mu/\rho_s D_\infty$ is the Schmidt number, i.e. the ratio of momentum diffusivity to mass diffusivity. In both cases, ρ_s is the solvent density and μ is the solvent viscosity.

2.2. Osmotic reflection coefficient

The osmotic reflection coefficient for slit pores can be derived in an analogous method to cylindrical pores [15]. The Gibbs-Duhem equation describes thermodynamic equilibrium within the pore as

$$\frac{\partial P}{\partial x} = - c\,(x, z)\, \frac{\partial E}{\partial x}, \quad \text{Eq 7}$$

which states that the lateral (x direction) pressure gradient must be balanced by a solute chemical potential gradient at a given axial (z direction) position. Here, E represents the energy at a given position. We further make the assumption that the Boltzmann equation is valid such that $c(x,z) = c_o(z)\exp[-(E(x)-E(0))/kT]$, where c_o is the concentration at the pore centerline, k *is the* Boltzmann constant, and T is temperature. If we assume that the x and z components of the solute potential can be separated, incorporating this expression into Eq 7 yields

$$P\,(x, z) = P\,(0, z) - c_o\,(z)\, RT \left[1 - exp \left(- \left(\frac{E\,(x) - E\,(0)}{kT} \right) \right) \right] \quad \text{Eq 8}$$

where R is the universal gas constant. The Navier-Stokes equations for fluid transport can be used to solve for the velocity profile within a single membrane pore

$$\frac{\partial P}{\partial z} = \mu \frac{\partial^2 v_z}{\partial x^2} \quad \text{Eq 9}$$

where μ is the solvent viscosity and v_z is the velocity in the z direction. Note that Eq 9 neglects the effects of counterelectroosmosis arising from the electrical stresses in the fluid. Combining Eq 8 and Eq 9, we obtain

$$\mu\frac{\partial^2 v_z}{\partial x^2}=-\frac{dP\left(0,z\right)}{dz}+\frac{dc_o\left(z\right)RT}{dz}\left[1-exp\left(-\left(\frac{E\left(x\right)-E\left(0\right)}{kT}\right)\right)\right] \quad \text{Eq 10}$$

Application of the appropriate boundary conditions yields an expression for the velocity at a given position relative to the pore centerline:

$$v_z=-\frac{dP_o\left(z\right)}{2\mu dz}\left(h^2-x^2\right)+\frac{d\pi_o\left(z\right)}{2\mu dz}\left(h^2-x^2\right)-e^{E(0)/k_BT}\frac{d\pi_o\left(z\right)}{\mu dz}\int_x^h dx'\int_0^{x'}[e^{-E\left(x''\right)/k_BT}]dx''.$$

Eq 11

where h is the pore half width and $\pi_o = c_oRT$ is the osmotic pressure. In order to determine the solvent flux through the pore, the velocity is averaged over the entire pore width, resulting in

$$\langle v_z\rangle=-\frac{dP_o\left(z\right)h^2}{3\mu dz}+\frac{d\pi_o\left(z\right)h^2}{3\mu dz}-\frac{e^{E(0)/k_BT}}{h}\frac{d\pi_o\left(z\right)}{\mu dz}\int_0^h dx\int_x^h dx'\int_0^{x'}\left[e^{-E\left(x''\right)/k_BT}\right]dx''. \quad \text{Eq 12}$$

Since Eq 12 is written in terms of intrapore concentrations and pressures, these values must be transformed into values just outside the pore entrance through relations as described in Anderson et al [15]

$$\pi_o\left(0\right)=\pi_{o,\infty}e^{-E(0)/k_BT} \quad \text{Eq 13 (a)}$$

$$\pi_o\left(L\right)=\pi_{L,\infty}e^{-E(0)/k_BT} \quad \text{Eq 13 (b)}$$

$$P_o\left(0\right)=P_{o,\infty}-\pi_{o,\infty}+\pi_{o,\infty}e^{-E(0)/k_BT} \quad \text{Eq 13 (c)}$$

$$P_o\left(L\right)=P_{L,\infty}-\pi_{L,\infty}+\pi_{L,\infty}e^{-E(0)/k_BT} \quad \text{Eq 13 (d)}$$

If we non-dimensionalize the pore position and solute radius (r_s) by the pore half width we get $\rho = x/h$ and $\lambda = r_s/h$, respectively. Finally, substituting Eq 13 into Eq 12 and rearranging we obtain an expression for the water flux through each slit pore

$$v = \frac{h^2}{3\mu L}\left(\Delta P - \sigma \Delta \pi\right)$$

$$\text{where } \sigma = 1 - 3\int_0^1 d\rho \int_\rho^1 d\rho' \int_0^{\rho'} \left[e^{-E\left(\rho''\right)/k_B T} \right] d\rho''. \qquad \text{Eq 14}$$

The impact of the osmotic reflection coefficient may be particularly important in systems where the solute concentration is relatively high. In systems where solute concentrations are low, the osmotic reflection coefficient has no effect on the filtrate flux because the contribution from solute osmotic pressure is negligible. This simplifies the model considerably and may have relevance in a number of filtration modalities.

2.3. Partition coefficient

The partition coefficient for a slit pore is the ratio of the bulk membrane surface concentration just outside the pore to the average concentration just inside the pore $\langle c_o \rangle$ [5],

$$\phi = \frac{\langle c_o \rangle}{c_{b,m}} = \int_0^{1-\lambda-(d_o/h)} g\left(\rho\right) d\rho \qquad \text{Eq 15}$$

where $g(\rho)$ is the potential function at some non-dimensional position ρ is the Born in the pore and d_o is the Born repulsion limit of approximately 0.187 nm [16]. Note that the upper limit of the integration in Eq 15 is less than unity due to steric hindrance and Born repulsion effects. In other words, there is a restriction that the solute center cannot sample all positions within the pore since the solute itself cannot pass through the pore wall. For the case where LW, AB, and EL interactions are neglected, the partition coefficient depends only on steric considerations such that $\phi = 1-\lambda-(d_o/h)$. The potential function can be represented by a Boltzmann distribution through $g(\rho)=\exp(-E(\rho)/kT)$, where $E(\rho)$ is the energy at a given non-dimensional pore position [5].

2.4. Hindrance factors

The diffusive and convective hindrance factors can be calculated through existing correlations for the transport of solutes through slit pores [17]. These correlations exist for both centerline positions and cross-sectionally averaged off-axis positions. Since repulsive interactions between solute and membrane are likely to position solutes closer to the pore centerline, we apply the centerline approximation in this study. The centerline hindrance factors are calculated through [17]

$$K_c = \frac{1}{2}\left(3-(1-\lambda)^2\right)\left(1-\frac{\lambda^2}{3}\right) \quad \text{Eq 16}$$

$$K_d = 1 - 1.004\lambda + 0.418\lambda^3 + 0.21\lambda^4 - 0.169\lambda^5 \quad \text{Eq 17}$$

which are valid up to approximately $\lambda = 0.5$.

2.5. Surface element integration for slit pores

In order to determine the impact of LW, AB, and EL interactions on transport, the interaction energy between the solute and membrane surface (or pore wall) must be calculated. This energy has typically been determined through application of the Derjaguin approximation. However, as Bhattarcharjee at al [5] note, this approximation has been carefully validated only for sphere-sphere interactions. Therefore, an alternative approach, the surface element integration (SEI) method, is applied for the sphere-plane scenario discussed in this paper [5].

This method has been applied previously for circular pores and solutes approaching a plane from infinite distance, but not for a slit pore membrane geometry [18][19]. Therefore, we develop a mathematical framework for the slit pore geometry shown in Figure 2. Applying an approach similar to Bhattacharjee [15], we use cylindrical coordinates to describe the solute as a group of cylindrical disks, each with infinitesimal thickness, dr. The distance of a cylindrical disk from the solute origin is defined

$$d = r_s\sqrt{1-r^2/r_s^2} \quad \text{Eq 18}$$

where r is the radius of a differential area element ($dA = 2\pi r dr$) at some position d from the solute origin, and r_s is the solute radius. Using Eq 18, we can determine the distance of a differential area from the pore wall (L) by accounting for the pore width and the position of the solute laterally within the pore, such that

$$L_{ABC} = h - x - d\sqrt{1-r^2/r_s^2} \quad \text{Eq 19}$$

Eq 19 provides the distance of a differential area with the pore wall closest to the half sphere ABC. For the half sphere closest to the opposite pore wall, the distance is

$$L_{AB'C} = h - x + d\sqrt{1-r^2/r_s^2} \quad \text{Eq 20}$$

Integrating over the entire sphere at a given position results in the following expression

$$E(r) = 2\pi \int_0^{r_s} \Delta G \left(h - x - r_s \sqrt{1 - r^2/r_s^2} \right) r dr + 2\pi \int_0^{r_s} \Delta G \left(h - x + r_s \sqrt{1 - r^2/r_s^2} \right) r dr \quad \text{Eq 21}$$

which is the energy for the solute at a given position within the pore. However, each force is a function of the distance between the pore surface and solute surface element; thus, the interaction energy will also vary with distance as follows

$$\Delta G^{LW}(L) = -A/12\pi L^2 \quad \text{Eq 22}$$

$$\Delta G^{AB}(L) = \Delta G_o^{AB} exp\left(\frac{d_o - L}{D}\right) \quad \text{Eq 23}$$

$$\Delta G^{EL}(L) = 2\pi\varepsilon_o\varepsilon_r \left(\psi_1^2 + \psi_2^2\right) \left(1 - coth(\kappa L) + \frac{2\psi_1\psi_2}{\psi_1^2 + \psi_2^2} \mathrm{csch}(\kappa L)\right) \quad \text{Eq 24}$$

for LW, AB, and EL components, respectively. Here, L is the distance between two differential area elements A, is the Hamaker constant for Lifshitz van der Waals interactions, ΔG_o^{AB} is the AB interaction at contact, D is the AB decay length, ε_o is the vacuum permittivity, ε_r is the relative permittivity, ψ_1 and ψ_2 are the surface potentials of solute and membrane, and κ is the inverse Debye length. The Hamaker constant is itself a function of the LW free energy of interaction at contact such that $A = -12\pi d_o^2 \Delta G_o^{LW}$. The AB (hydration repulsion) force can exhibit oscillatory or monotonic decrease with distance depending on surface composition and roughness [20][21]. For the relatively rough polymer coated SNM surface used in our membranes, we assume monotonic decrease of the acid-base repulsion as shown in Eq 23. The value of the decay length can change due to the amount of surface bound water. Surfaces with either positive or negative charge can attract counterions to the interface, creating a hydration shell of water molecules, resulting in an increase in the decay length.

2.6. Determining LW and AB interaction components

The contribution of LW forces to the total interaction energy can be represented by the Hamaker constant, by the surface potential for electrostatics, and by the acid-base free energy of interaction for the acid-base force. While values for the surface potential of protein and membrane can be easily determined using literature data for surface charge and zeta potential, LW and AB forces are more difficult to determine experimentally. The van Oss-Good-Chaudhury (VCG) method can be applied in order to isolate the Hamaker constant

and the Gibbs free energy for acid-base interaction at contact using goniometric measurements. Briefly, this method assumes that the total surface tension (γ^T) of a solid or liquid is comprised of individual van der Waals (γ^{LW}), acid (γ^+), and base (γ^-) components. As the individual components are not known explicitly for the great majority of surfaces, the VCG method provides a framework for determining them experimentally using three liquids of known surface tension. Then, using thermodynamic combining relations, the surface tension values of the unknown surface can be calculated by solving

$$(1+cos\theta)\,\gamma_l^T = 2\left(\sqrt{\gamma_m^{LW}\gamma_l^{LW}} + \sqrt{\gamma_m^+\gamma_l^-} + \sqrt{\gamma_m^-\gamma_l^+}\right) \quad \text{Eq 25}$$

$$(1+cos\theta)\,\gamma_l^T = 2\left(\sqrt{\gamma_s^{LW}\gamma_l^{LW}} + \sqrt{\gamma_s^+\gamma_l^-} + \sqrt{\gamma_s^-\gamma_l^+}\right) \quad \text{Eq 26}$$

where Eq 25 applies for the membrane and Eq 26 applies for the solute of interest [16]. Here, θ is the contact angle between the liquid and membrane or solute, and the subscripts *l*, *m*, and *s* represent the liquid, membrane, and solute, respectively. Applying Eq 25 and Eq 26 using three probe liquids (each with different γ_l values) results in a system of equations which, when solved, yield the individual LW and AB surface tension parameters. Finally, these surface tension parameters can be used to determine the interaction energy at contact between the solute and membrane as follows [16]

$$\Delta G_o^{LW} = 2\left[\sqrt{\gamma_s^{LW}} - \sqrt{\gamma_l^{LW}}\right]\left[\sqrt{\gamma_l^{LW}} - \sqrt{\gamma_m^{LW}}\right] \quad \text{Eq 27}$$

$$\Delta G_o^{AB} = 2\left[\sqrt{\gamma_l^+}\left(\sqrt{\gamma_s^-} + \sqrt{\gamma_m^-} - \sqrt{\gamma_l^-}\right) + \sqrt{\gamma_l^-}\left(\sqrt{\gamma_s^+} + \sqrt{\gamma_m^+} - \sqrt{\gamma_l^+}\right) - \sqrt{\gamma_s^+\gamma_m^-} - \sqrt{\gamma_s^-\gamma_m^+}\right]$$

Eq 28

3. Experimental Methods

3.1. Solute selection

B2M is of particular interest in this study due to its molecular dimensions (MW 11800), which allow for partial sieving at SNM pore sizes (r_s = 1.59 nm) [13]. Partial sieving will allow us to elucidate the effects of XLDVO interactions between solute and pore. Furthermore, since B2M has been heavily researched as a kidney function middle molecular weight marker, there is published data available on its electrostatic properties [22].

3.2. Membrane fabrication

The fabrication of SNM is detailed extensively in other published work [8]. Briefly, microelectromechanical systems (MEMS) fabrication techniques are applied to grow a thin silicon oxide sacrificial layer on a silicon substrate. Upon etching of the oxide, nanometer scale pores are formed in the membrane. Virgin SNM have a roughly 11 nm pore size, and to facilitate membrane handling, membranes are fabricated with 0.95% surface porosity and a thickness of 400 nm. The porosity is precisely known since the photolithographic mask results in exactly 4.343×10^5 pores/mm^2.

In order to prevent protein adhesion and pore blocking of the membrane during filtration, membranes are further functionalized through silane chemistry [8]. SNM were immersed in 2 % w/v polyethylene glycol (PEG) silane (Gelest) dissolved in 75 mL of toluene for 2 hr at 70 °C. Following PEG treatment, the membrane pore size decreased from roughly 11 nm to 6 nm and water constant angles stabilized at 35 – 40 degrees, suggesting significant surface modification. The evaluation of the membrane pore size is discussed in more detail subsequently. Pure water permeability experiments on PEG-coated membranes showed linear increases in flux with applied pressure, suggesting a consistent pore size and uniform coverage of PEG within the membrane pores.

3.3. Solute filtration experiments

Filtration experiments were conducted using a custom experimental setup. A syringe pump (KD Scientific Inc, #KDS200) was used to pressurize a reservoir containing the feed solution. A peristaltic pump (Cole Palmer Masterflex, #7551-00) provided fluid flow (2 ml/min) through a pressure transducer (Omega Engineering Inc, #PX429) and specially designed aluminum flow cell. Experiments were automated using a connected computer, with hydraulic pressures taken over a range from 3 to 55 kPa (0.5 to 8 psi), which includes the typical physiological arterial pressure (~13.8 kPa). Aluminum tubing (McMaster-Carr, #5177K61) was used to attach the different system components and to prevent significant protein adsorption. The experimental system was assembled and sterilized by autoclave before each set of experiments. B2M (Lee Biosolutions Inc, #126-11) was dissolved in divalent cation-free phosphate buffered solution (UCSF Cell Culture Facility), and B2M immunoassays (performed on the SPA Plus, The Binding Site) were conducted at the UCSF Clinical Chemistry Laboratory in order to determine the solute concentrations in feed and filtrate.

3.4. Membrane pore size measurements

Membrane pore sizes were determined before filtration experiments through hydraulic permeability measurements using a feed solution of pure water. SNM were placed in the testing flow cell and subjected to feed hydraulic pressures of 1, 2, and 4 psi (6.9, 13.8, and 27.6 kPa). The filtrate volume collected over a time interval was weighed in order to determine the water flux across the membrane at a given pressure. Using this water flux (Q) data, the membrane surface porosity, membrane area (A_m) and known membrane thickness, the SNM slit half-width was then back-calculated using the follow equation:

$$h=0.5\sqrt{(8\mu\delta_m Q/\varepsilon A_m \Delta P)}, \quad \text{Eq 29}$$

which is derived from the Navier-Stokes equation for flow through a slit pore. As stated earlier, ε represents the membrane porosity, which is itself a function of the known pore number, pore length, and slit width h. The porosity can be represented through $\varepsilon = 2NhL/A_m$, where L is pore length and N is the number of pores. The "effective" pore size is then determined through Eq 29 by incorporating the line of best fit for the water flux versus pressure data. For a membrane of a constant, known geometry (in this case, a slit pore), the pore size should not change across all tested pressures.

Using Eq 29, we determined the post-PEGylation membrane pore sizes as 6.1 ± 0.2 nm and 6.3 ± 0.2 nm for the two membranes used in this study. The reduced pore size necessarily results in a decrease in the membrane surface porosity. For pore sizes in this range, there is complete rejection of albumin as confirmed by previous studies [23][24][8]. This method assumes that the PEG chains grafted on the membrane pore surface form a uniform, dense structure and the large majority of the fluid flows in the open pore region. With this assumption, polymer chain compression is likely to be limited due to the steric constraints arising from adjacent chains. Thus, the PEG polymer chains form an effective "hard wall" when modeled with Eq 29.

3.5. Solute and membrane characterization

Contact angle measurements were conducted on both PEG-coated SNM and B2M samples using a commercially available goniometer (Biolin Scientific, Theta Lite). To prepare the B2M for goniometric analysis, a sample of B2M (10 mg) in 30 mL of solution was filtered at 140 kPa (20 psi) onto 5 kDa ultrafiltration membranes (Sterlitech Corp, Trisep UF5) placed in a stirred ultrafiltration cell (Amicon, 8050). Before filtration, each membrane was compacted at the operating pressure in order to prevent passage of solute through the membrane. Once the B2M solution was filtered onto the Trisep membrane, excess surface moisture was allowed to evaporate (approximately 30 minutes). Contact angles for water, diiodomethane (Sigma Aldrich, #158429), and ethylene glycol (Sigma Aldrich, #85978) were then measured on the hydrated protein layer. Further details about the procedure for performing these measurements is available in the literature [25] [16]. Electrostatic parameters for the B2M [22] and PEG-coated SNM [26] are sourced from the literature.

4. Results and Discussion

4.1. B2M and PEG-SNM parameters

As discussed above, B2M and PEG-SNM surface tension parameters were determined through contact angle analysis. Table 1 summarizes the surface tension parameters, interaction energy constants, and feed solution conditions. Comparing the B2M surface tension parameters to those for hydrated human serum albumin (HSA, from literature) [16], B2M exhibits a greater overall contribution from LW forces and a slightly lower polar AB component. B2M possesses similar LW and polar AB components to Immunoglobulin G

(IgG, from literature) [16], but exhibits less apolar AB activity. The similarity to IgG is not surprising, as the amino acid sequence homology of B2M is related to the Ig constant domain [27]. PEG-SNM surface tension values reported here are similar to values for PEG reported in the literature [16]. Since the PEG-SNM is also highly polar, this results in large Gibbs free energy at contact with B2M. Similarly, as the PEG-SNM also possesses a large LW component, the Hamaker constant is high for the PEG-SNM/B2M pair. Note that the surface potential for B2M is significantly lower than that for BSA (−20 mV, from literature) [5]. Therefore, there is less EL repulsion between B2M and PEG-SNM than there would be for a hypothetical BSA/PEG-SNM pair [16]. The high ionic strength of the feed solution also limits the contribution of EL forces due to double layer shielding.

4.2. Model output

4.2.1. Interaction energy across pore—It is important to first consider the effect that each individual interaction energy component has on the total interaction between solute and membrane pore. The interaction energy (normalized by kT) for different positions relative to the pore centerline is shown in Figure 4 for LW, AB, and EL interactions. Here, the position relative to the centerline is a function of the pore half width, solute radius, and Born repulsion limit, such that $x_r = 1-\rho-d_o/h$. Three pore half-widths are modeled, and in each case B2M is taken as the solute of interest. It is clear from the results that the biggest contribution to the interaction energy is the AB interaction. This is expected given the large value for AB interaction at contact between B2M and PEG-SNM as determined by contact angle measurements. As the solute moves farther from the closest point of contact, it rapidly approaches the opposing pore wall. Note that we use a decay length $D = 0.1$ nm for the acid-base interaction. Decay length values from literature are typically in the range of 0.1 to 0.6 nm, and we selected from the lower end of this range due to the non-ionic nature of the PEG-based coating on the SNM [28]. Hydrophilic coatings with ionic constituents, such as zwitterions, can demonstrate much larger decay lengths due to the larger hydration shell around these moieties.

There is a considerably lower impact from LW and EL forces for the interaction of B2M and the PEG-SNM near the pore wall. However, since the AB interaction decays relatively quickly with $D = 0.1$ nm, the contribution of LW forces at the pore centerline remains much closer to the value at contact than for AB forces. For EL interactions, there is an almost negligible contribution to the interaction energy for all three pore sizes. This is a consequence of the small net charge on B2M at physiological pH in buffered solution. Proteins with a much greater net charge, such as albumin, will exhibit greater electrostatic repulsion, especially in cases where the pore wall itself is adsorbed with albumin. In non-physiological medium, such as very dilute salt solutions, the increased Debye length will result in a greater EL contribution.

It should be noted that the EL interaction does not appear to be monotonic close to the pore wall. This is the result of the behavior of the Debye-Huckel equation (Eq 24), which as presented is solved for the case of constant surface potential (CP). It has been shown previously that the behavior of the electrostatic force is markedly different when solved at CP compared to that at constant surface charge (CC) [29]. This discrepancy is particularly

pronounced when the difference between the potentials of interacting surfaces is relatively large, with the more strongly charged surface inducing an opposite charge on the other surface at small separations. Note that the "actual" interaction between the solute and pore is likely somewhere between the CP and CC solutions. Due the limited impact of EL interactions in our modeled scenario, we apply the CP case and assume that any deviations are minor relative to the AB and LW contributions.

4.2.2. Partition coefficient—As discussed earlier, the partition coefficient is a function of the integrated interaction energy over the pore width. Figure 5 shows the partition coefficient for a range of λ values (at constant r_s= 1.59 nm for B2M) for different values of the AB decay constant. For the steric only condition, it is clear that ϕ decreases as the solute radius approaches the pore half width. As the AB decay constant increases, ϕ is shifted lower for a given λ value. At these larger decay constant values, the partition coefficient is essentially zero for even moderate values of λ. In practical terms, this means that shifting the AB decay constant through attachment of different modifiers to the silicon surface could be beneficial or detrimental to filtration performance. For example, in order to limit solute transmission, zwitterionic polymers with large AB decay constants could be covalently attached to the membrane. On the other hand, lower decay constant polymers such as PEG will only mildly prohibit sieving compared to that predicted based only on the steric exclusion. Note that, although certain surface modifiers such as zwitterionic polymers may have increased AB decay constants, there may be resultant increases in LW and EL contributions as well.

4.2.3. Osmotic reflection coefficient—Like the partition coefficient, the osmotic reflection coefficient is a function of the interaction energy between the membrane and solute. As the solute radius approaches the pore half width, σ increases monotonically (Figure 6). It is clear from the model output that increasing the AB decay constant results in a much faster rise in σ at low values of λ. In this study, the osmotic reflection coefficient is unlikely to have a significant impact on sieving since the feed B2M concentration is relatively low. However, filtration of blood or analogous fluids with particularly high concentrations of certain proteins might exhibit decreased solvent flux compared to the pure water case. While the partition coefficient approaches zero at large D for relatively small values of λ, the osmotic reflection coefficient only approaches unity at large and λ. This behavior results from the differences in the way each parameter is calculated, with ϕ and σ requiring single and triple integration of the interaction energy, respectively.

4.2.4. Observed and actual sieving coefficients for B2M—Figure 7 depicts the modeled change in the observed and actual sieving coefficients for a variety of pore sizes. These simulations incorporate the hindrance factors described earlier (Eq 16 and Eq 17), which account only for steric effects. Note that the observed and actual sieving coefficients both initially decrease with increasing pressure, but exhibit different behavior at higher pressure. As convection begins to dominate diffusion at higher pressures, the actual sieving coefficient approaches its asymptotic value (at infinite convection). However, as convection dominates, concentration polarization causes a higher concentration of solute in solution at the feed-side membrane interface. Therefore, since the bulk solute concentration is relatively constant and lower than the increasingly higher interface concentration, the observed (or

"apparent") sieving coefficient increases to unity at higher pressures. Experimental validation for the minimum in the observed sieving coefficient at intermediate flux is available in the literature [3].

4.3. Comparison with experimental data

Experiments were conducted for B2M sieving using two membranes with different pore sizes after PEGylation (6.1 nm and 6.3 nm). With the exception of a data point at 1 psi for the membrane with 6.1 nm pore size, the experimental data match the XDLVO model well (Figure 8). The experimental data are also noticeably lower than predictions of the steric only model, which neglects the interaction energy between the pore and solute. Given the small net charge of B2M, the reduction in transmission compared to that predicted by the steric model is predominantly due to LW and AB interactions and their impact on the partition coefficient. Therefore, DLVO models, which inherently neglect these interactions, would have significantly overestimated the experimental sieving data. In our experiments the pure water and protein solution water permeability were approximately the same over all tested pressures, indicating that membrane fouling is unlikely to be responsible for the difference between the steric only and the XDLVO model predictions. This suggests that experimental and model differences are not the result of membrane changes resulting from pore occlusion by proteins. Note that the model predictions are calculated for $D = 0.11$ nm, which here acts a fitting parameter to model data for both membrane pore sizes tested. We believe this to be a reasonable value for the AB decay constant and consistent with the range of values predicted in the literature (see earlier discussion, Section 4.2.1). A shift in the value for D will indeed alter the model fit and agreement with experimental data.

5. Conclusion and Future work

The purpose of this work was to evaluate the accuracy of the XDLVO model for membrane transport using slit pore SNM with uniform pore size and surface porosity. Equations for the partition coefficient and osmotic reflection coefficient for slit pore membranes were developed accounting for LW, AB, and EL interactions using surface element integration. The results of the work demonstrate that the models can be used to accurately predict the sieving of B2M, a particularly relevant middle molecular weight molecule in applications of the artificial kidney.

A key conclusion of this work is that AB repulsion between solute and membrane can cause a marked decrease in the sieving coefficient of B2M. While the reduction in sieving coefficient due to XLDVO interactions is fairly small for the AB decay constant applied here (approximately 10–20%), other surface modifiers such as zwitterionic polymers (with larger decay constant) could cause a much more pronounced reduction in solute transmission.

The implications of this work for the design of biomedical devices and other processes are significant and should be investigated in future studies. If solutes are intended to be excluded from pores, large decay constant hydrophilic polymers could be grafted to the pore walls, allowing one to use membranes with larger pore size to maximize water permeability while still retaining the solutes of interest. On the other hand, if the aim is to increase solute transmission through the pores, polymers with small decay constants would facilitate

penetration of solutes into the pores. Ultimately, this paper validates a model that can serve as a valuable tool in demonstrating how SNM can be optimized to achieve the desired removal of clinically relevant middle molecular weight solutes.

Acknowledgments

We would like to thank the National Institutes of Health (NIH) for funding this research work through the following grants: R01EB014315 and U01EB021214, both of which were provided through the National Institute of Biomedical Imaging and Bioengineering (NIBIB).

References

1. Wang J, Dlamini DS, Mishra AK, Pendergast MTM, Wong MCY, Mamba BB, Freger V, Verliefde ARD, Hoek EMV. A critical review of transport through osmotic membranes. J Memb Sci. 2014; 454:516–537.
2. Dechadilok P, Deen WM. Electrostatic and electrokinetic effects on hindered convection in pores. J Colloid Interface Sci. 2009; 338:135–144. [PubMed: 19589534]
3. Opong W, Zydney A. Diffusive and convective protein transport through asymmetric membranes. AIChE J. 1991; 37:1497–1510.
4. Langsdorf LJ, Zydney AL. Diffusive and convective solute transport through hemodialysis membranes: a hydrodynamic analysis. J Biomed Mater Res. 1994; 28:573–582. [PubMed: 7517941]
5. Bhattacharjee S, Sharma A, Bhattacharya P. Estimation and influence of long range solute. Membrane interactions in ultrafiltration. Ind Eng Chem Res. 1996; 35:3108–3121.
6. Quinn JA, Anderson JL, Ho WS, Petzny WJ. Model pores of molecular dimension: The preparation and characterization of track-etched membranes. Biophys J. 1972; 12:990–1007. [PubMed: 4339801]
7. Mitchell BD, Deen WM. Effect of concentration on the rejection coefficients of rigid macromolecules in track-etch membranes. J Colloid Interface Sci. 1986; 113:132–142.
8. Fissell WH, Dubnisheva A, Eldridge AN, Fleischman AJ, Zydney AL, Roy S. High-performance silicon nanopore hemofiltration membranes. J Memb Sci. 2009; 326:58–63. [PubMed: 20054402]
9. Fissell WH, Roy S, Davenport A. Achieving more frequent and longer dialysis for the majority: wearable dialysis and implantable artificial kidney devices. Kidney Int. 2013; 84:256–64. [PubMed: 23407434]
10. Smith RA, Goldman K, Fissell WH, Fleischman AJ, Zorman CA, Roy S. Removal of endotoxin from deionized water using micromachined silicon nanopore membranes. J Micromechanics Microengineering. 2011; 21
11. Gierak J, Madouri A, Biance AL, Bourhis E, Patriarche G, Ulysse C, Lucot D, Lafosse X, Auvray L, Bruchhaus L. Sub-5nm FIB direct patterning of nanodevices. Microelectron Eng. 2007; 84:779–783.
12. Tong HD, Jansen HV, Gadgil VJ, Bostan CG, Berenschot E, van Rijn CJM, Elwenspoek M. Silicon nitride nanosieve membrane. Nano Lett. 2004; 4:283–287.
13. Cheung AK, Rocco MV, Yan G, Leypoldt JK, Levin NW, Greene T, Agodoa L, Bailey J, Beck GJ, Clark W. Serum β-2 microglobulin levels predict mortality in dialysis patients: results of the HEMO study. J Am Soc Nephrol. 2006; 17:546–555. [PubMed: 16382021]
14. Schock G, Miquel A. Mass transfer and pressure loss in spiral wound modules. Desalination. 1987; 64:339–352.
15. Anderson JL, Malone DM. Mechanism of osmotic flow in porous membranes. Biophys J. 1974; 14:957–982. [PubMed: 4429773]
16. Van Oss, CJ. Interfacial forces in aqueous media. CRC press; 2006.
17. Dechadilok P, Deen WM. Hindrance factors for diffusion and convection in pores. Ind Eng Chem Res. 2006; 45:6953–6959.

18. Bhattacharjee S, Elimelech M. Surface element integration: a novel technique for evaluation of DLVO interaction between a particle and a flat plate. J Colloid Interface Sci. 1997; 193:273–285. [PubMed: 9344528]

19. Bhattacharjee S, Chen JY, Elimelech M. DLVO interaction energy between spheroidal particles and a flat surface. Colloids Surfaces A Physicochem Eng Asp. 2000; 165:143–156.

20. Donaldson SH, Valtiner M, Gebbie MA, Harada J, Israelachvili JN. Interactions and visualization of bio-mimetic membrane detachment at smooth and nano-rough gold electrode surfaces. Soft Matter. 2013; 9:5231–5238.

21. Israelachvili, JN. Intermolecular and surface forces: revised third edition. Academic press; 2011.

22. Ohhashi Y, Kihara M, Naiki H, Goto Y. Ultrasonication-induced amyloid fibril formation of β2-microglobulin. J Biol Chem. 2005; 280:32843–32848. [PubMed: 16046408]

23. Kim S, Feinberg B, Kant R, Chui B, Goldman K, Park J, Moses W, Blaha C, Iqbal Z, Chow C, Wright N, Fissell WH, Zydney AL, Roy S. Diffusive Silicon Nanopore Membranes for Hemodialysis Applications. PLoS One. 2016; 11

24. Song S, Faleo G, Yeung R, Kant R, Posselt AM, Desai TA, Tang Q, Roy S. Silicon nanopore membrane (SNM) for islet encapsulation and immunoisolation under convective transport. Sci Rep. 2016; 6

25. Absolom DR, van Oss CJ, Zingg W, Neumann AW. Determination of surface tensions of proteins II. Surface tension of serum albumin, altered at the protein-air interface. Biochimica et Biophysica Acta (BBA)-Protein Structure. 1981; 670:74–78.

26. Datta S, Conlisk AT, Kanani DM, Zydney AL, Fissell WH, Roy S. Characterizing the surface charge of synthetic nanomembranes by the streaming potential method. J Colloid Interface Sci. 2010; 348:85–95. [PubMed: 20462592]

27. Becker JW, Reeke GN. Three-dimensional structure of beta 2-microglobulin. Proc Natl Acad Sci U S A. 1985; 82:4225–4229. [PubMed: 3889925]

28. Kanduč M, Schlaich A, Schneck E, Netz RR. Hydration repulsion between membranes and polar surfaces: Simulation approaches versus continuum theories. Adv Colloid Interface Sci. 2014; 208:142–152. [PubMed: 24612664]

29. Gregory J. Interaction of unequal double-layers at constant charge. J Colloid Interface Sci. 1975; 51:44–51.

Highlights

- Silicon nanopore membranes are uniquely suited for transport model validation.
- Transport parameters, accounting for XDLVO interactions, are derived for slit pores.
- Acid-base repulsion causes a marked decrease in the solute sieving coefficient.
- The model serves as a valuable tool in optimizing sieving of biomolecules.

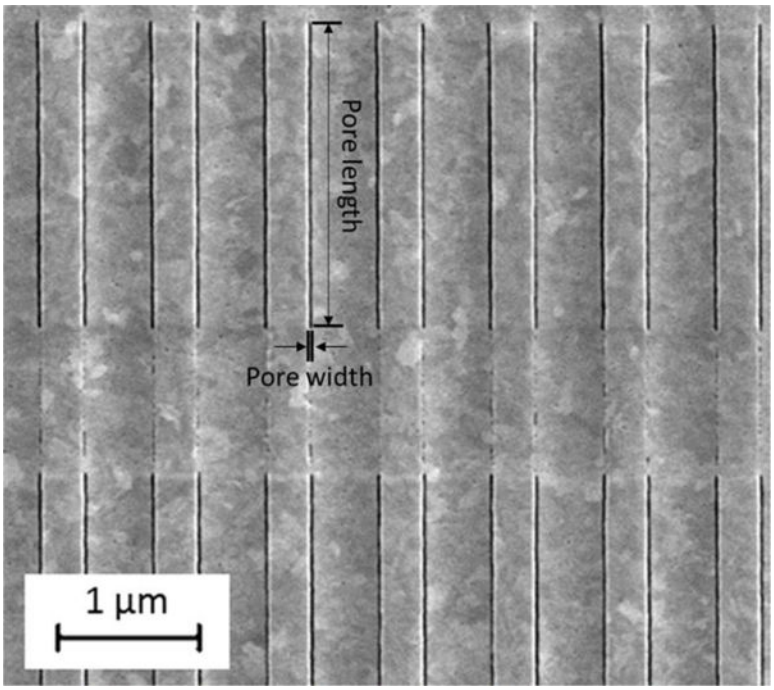

Figure 1.

Plan-view scanning electron microscopy (SEM) image of a typical SNM, depicting a 11 nm slit pore configuration, taken using a Carl Zeiss Ultra 55 field emission SEM. Pore width and length shown by hand superimposed on image.

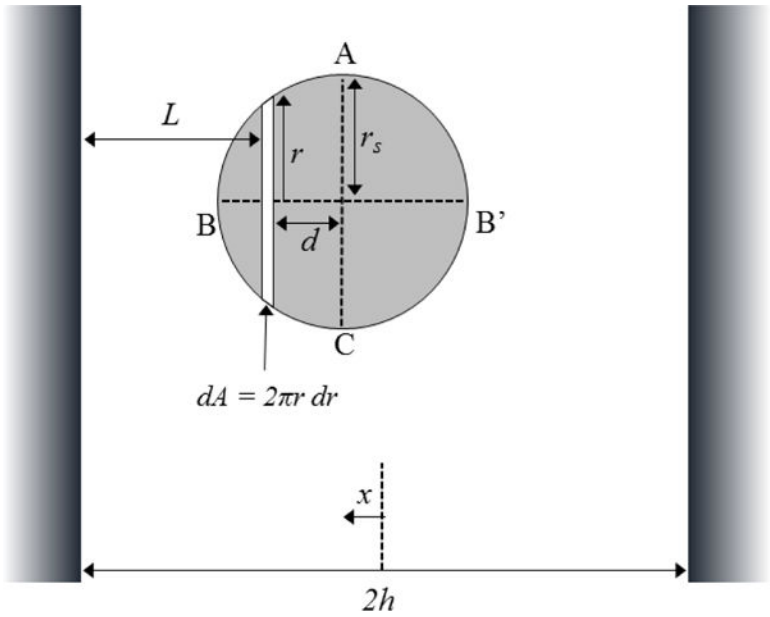

Figure 2.
Cross section graphical representation of solute positioned in slit pore.

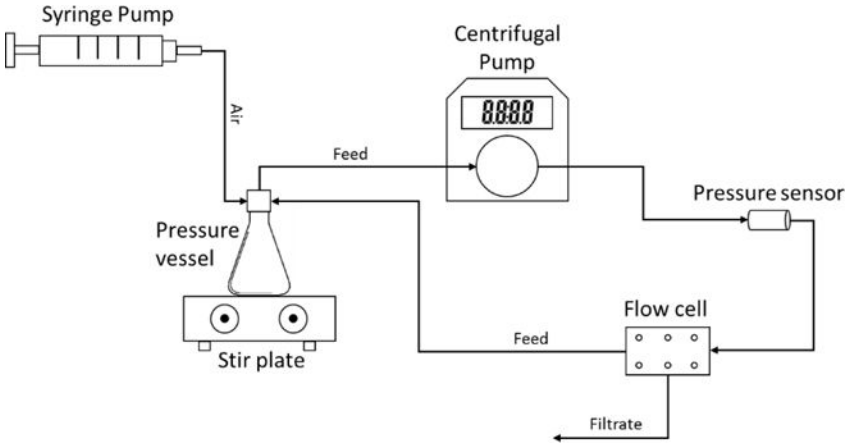

Figure 3.
Schematic of experimental setup.

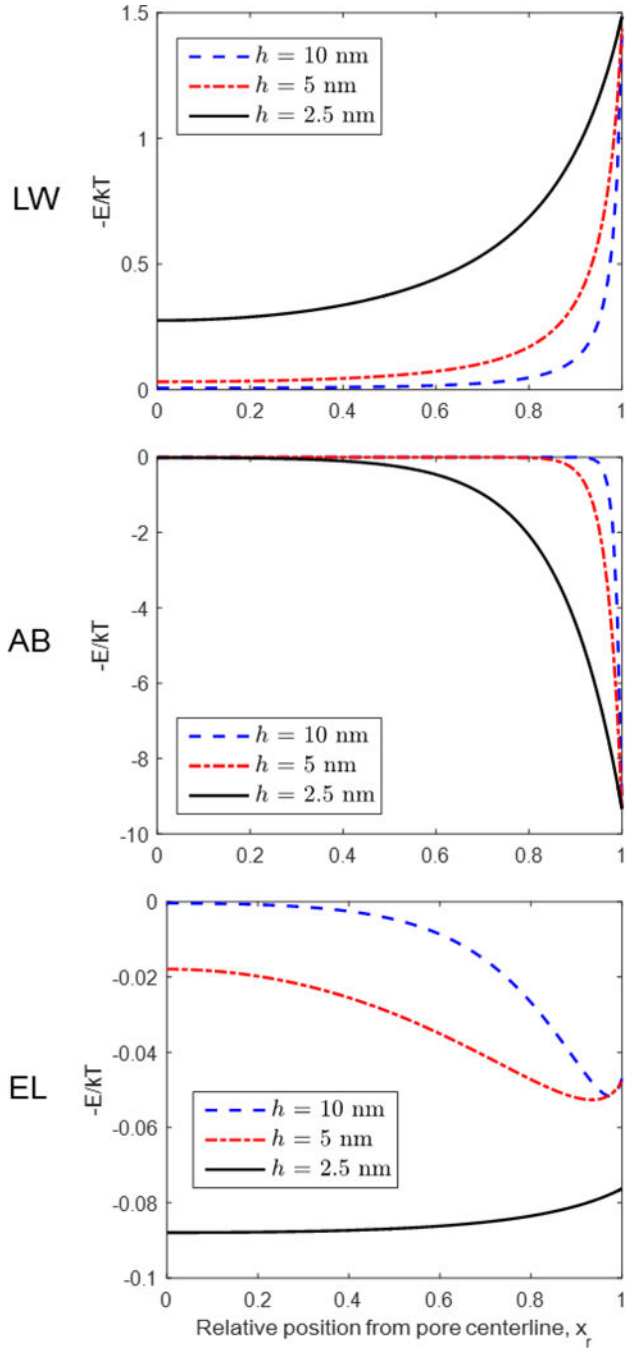

Figure 4.
Change in normalized interaction energy with relative position from pore centerline for LW (top), AB (middle), and EL (bottom) interactions, for three different pore half widths.

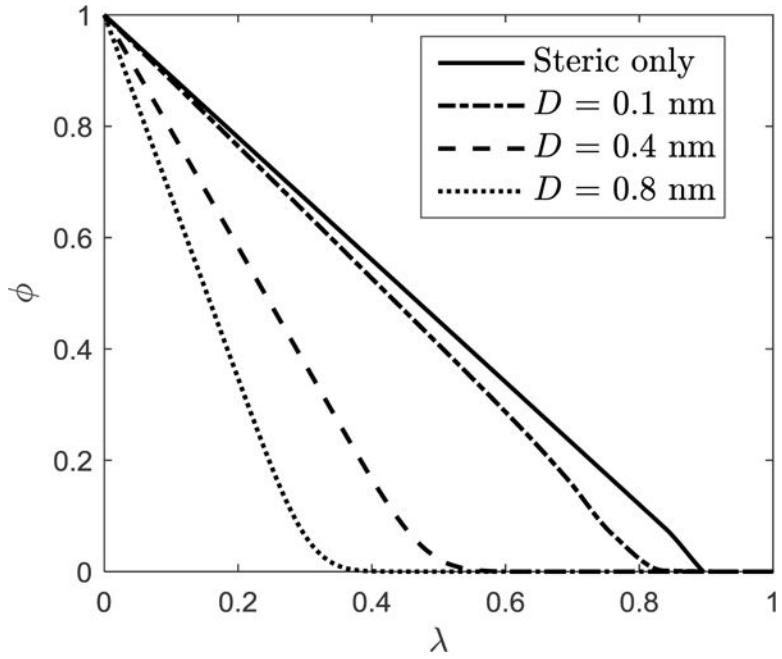

Figure 5.
Change in partition coefficient (ϕ) with increasing λ for the steric only case and for three AB decay constants.

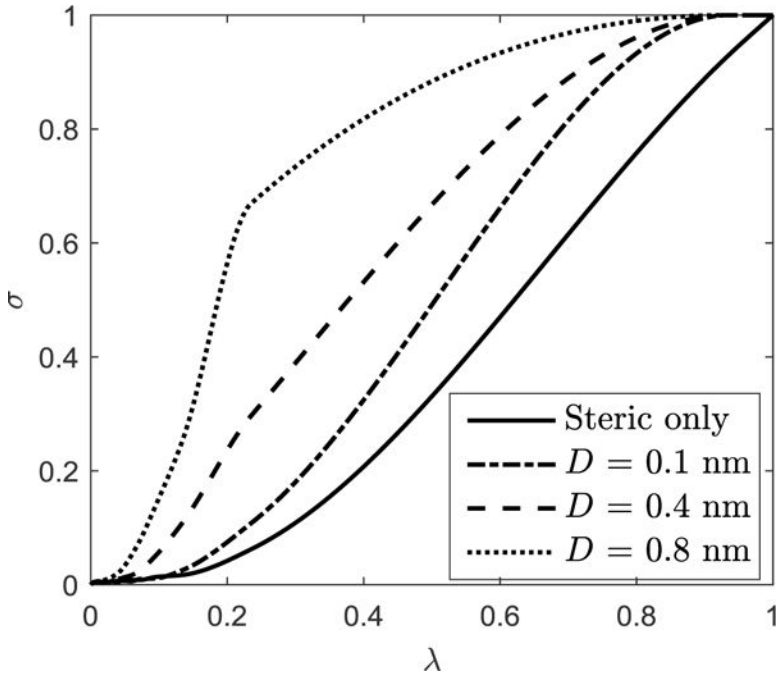

Figure 6.

Change in osmotic reflection coefficient (σ) with increasing λ for the steric only case and for three AB decay constants.

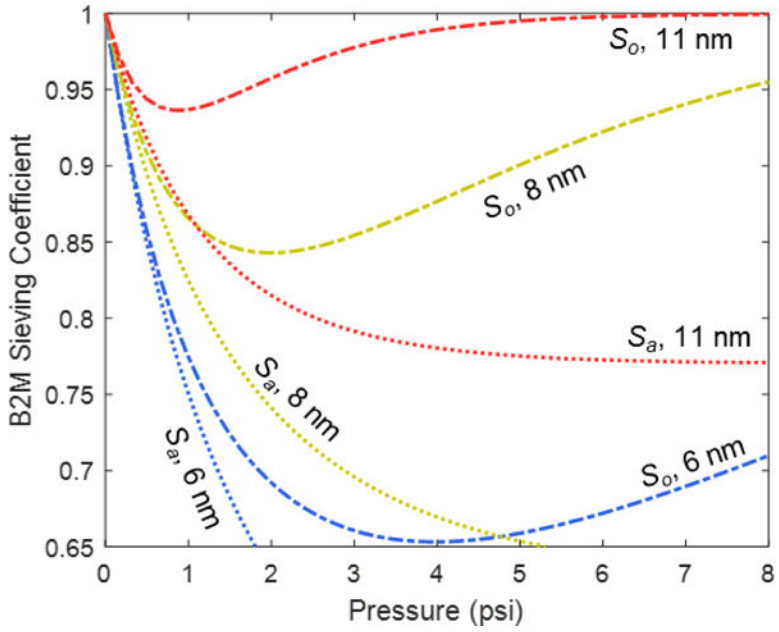

Figure 7.

Change in observed and actual sieving coefficients with increasing pressure for three pore sizes.

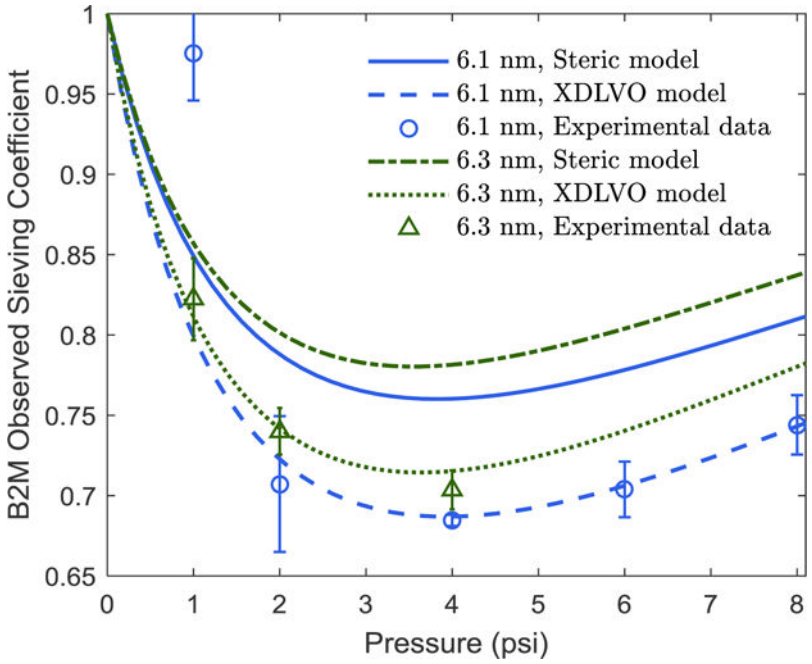

Figure 8.
Comparison of experimental data with model data for two different pore size membranes.

Table 1

Surface tension parameters as calculated from contact angles with three probe liquids, as well as interaction energy constants and feed solution parameters.

Surface tension parameters			
(*in mJ/m*^{2})	γ^{LW}	γ^+	γ^-
PEG-SNM	47	0	50.55
B2M	33.5	0	51
HSA (hydrated, literature)[1]	27.6	0.003	87.5
HSA (dry, literature)[1]	41.4	0.002	20
IgG (hydrated, literature)[1]	34	1.5	49.6
Interaction energy constants			
Hamaker Constant (A)	4.61×10^{-21}	J	
ΔG_o^{AB}	41	mJ/m^2	
Surface potential (B2M)[2]	−4	mV	
Surface potential (PEG-SNM)[3]	−12	mV	
Feed solution parameters			
pH	7.2		
Ionic strength	0.14	M	

[1] = [16],

[2] = [22],

[3] = [26]